

1 **Cytoplasmic delivery of quantum dots *via* microelectrophoresis** 2 **technique**

3 Mengke Han ^{1,2}, Jiangbo Zhao ^{1,2}, Joseph Mahandas Fabian ³, Samuel Evans ^{2,3}, Sanam Mustafa
4 ^{2,3}, Yinlan Ruan ^{1,2}, Steven Wiederman ^{2,3} and Heike Ebendorff-Heidepriem ^{1,2,*}

5
6 ¹ Institute for Photonics and Advanced Sensing (IPAS) and School of Physical Sciences, The University of
7 Adelaide, Adelaide, South Australia 5005, Australia.

8 ² ARC Centre of Excellence for Nanoscale BioPhotonics (CNBP), The University of Adelaide, Adelaide, South
9 Australia 5005, Australia.

10 ³ Adelaide Medical School, The University of Adelaide, Adelaide, South Australia 5005, Australia.

11 * Correspondence should be addressed to the following author:

12 Heike Ebendorff-Heidepriem (Professor)

13 School of Physical Sciences

14 Institute for Photonics and Advanced Sensing

15 The University of Adelaide, Adelaide, South Australia 5005, Australia

16 heike.ebendorff@adelaide.edu.au

17
18 **Keywords:** *Intracellular delivery, Microelectrophoresis, Nanoparticles, Quantum dots, Biosensor*

19
20
This is the peer reviewed version of the following article:

Han, M., Zhao, J., Fabian, J.M., Evans, S., Mustafa, S., Ruan, Y., Wiederman, S. and Ebendorff-Heidepriem, H.
(2021), Cytoplasmic delivery of quantum dots via microelectrophoresis technique. ELECTROPHORESIS, 42:
1247-1254.

which has been published in final form at <https://doi.org/10.1002/elps.202000388>. This article may be used for non-commercial purposes in accordance with Wiley Terms and Conditions for Use of Self-Archived Versions. This article may not be enhanced, enriched or otherwise transformed into a derivative work, without express permission from Wiley or by statutory rights under applicable legislation. Copyright notices must not be removed, obscured or modified. The article must be linked to Wiley's version of record on Wiley Online Library and any embedding, framing or otherwise making available the article or pages thereof by third parties from platforms, services and websites other than Wiley Online Library must be prohibited.

21 **Abstract:** Nanoparticles with specific properties and functions have been developed for various
22 biomedical research applications, such as *in vivo* and *in vitro* sensors, imaging agents and delivery vehicles
23 of therapeutics. The development of an effective delivery method of nanoparticles into the intracellular
24 environment is challenging and success in this endeavor would be beneficial to many biological studies.
25 Here, the well-established microelectrophoresis technique was applied for the first time to deliver
26 nanoparticles into living cells. An optimal protocol was explored to prepare semiconductive quantum dots
27 suspensions having high monodispersity with average hydrodynamic diameter of 13.2 - 35.0 nm.
28 Micropipettes were fabricated to have inner tip diameters of approx. 200 nm that are larger than quantum
29 dots for ejection but less than 500 nm to minimize damage to the cell membrane. We demonstrated the
30 successful delivery of quantum dots *via* small electrical currents (-0.2 nA) through micropipettes into the
31 cytoplasm of living human embryonic kidney cells (roughly 20 - 30 μm in length) using microelectrophoresis
32 technique. This method is promising as a simple and general strategy for delivering a variety of nanoparticles
33 into the cellular environment.

34 35 1 Introduction 36

37 The intracellular delivery of exogenous materials with high efficiency and specificity, has shown great
38 promise in deciphering and even modulating the complex, spatiotemporal interplay of biomolecules within
39 living cells [1,2]. As a powerful technique widely applied in modern biology, microelectrophoresis uses
40 electrical currents to eject charged substances through fine-tipped glass micropipettes into living cells [3].
41 Microelectrophoresis performs intracellular delivery in a highly controlled manner. It can limit the problematic
42 diffusion of chemically and pharmacologically active substances from micropipettes, by simply applying a
43 retaining current [3], which can reduce cell distortion and damage. In addition, as most biological membranes
44 *in vivo* maintain resting membrane potential differences ranging from -30 to -180 mV [4], microelectrophoresis
45 can readily locate target cells deep in tissue slice or living animals. Once the micropipette is pierced into the
46 cytosol of target cell, it can measure intracellular electrical activity in real-time [5].
47

48 Although microelectrophoresis has been established since *circa* 1900 [6], no studies have been conducted
49 to explore the intracellular microelectrophoretic delivery of nanoparticles, despite the rapid development of
50 utilizing nanomaterials in various intracellular biological research and medical applications [2]. For example,
51 fluorescent semiconductive quantum dots (QDs) with superior optical properties and surface groups permit
52 real-time tracking of intracellular molecules over time scales of milliseconds to hours, offering a capability to
53 monitor intracellular events that cannot be accomplished via organic fluorophores. The main challenge
54 confronting microelectrophoretic delivery of nanoparticles is the possibility of nanoparticle aggregation in the
55 tip of micropipettes during ejection, which can cause tip blockage and failed delivery. The reasons are twofold.
56

57 Firstly, traditionally used silver/silver chloride (Ag/AgCl) electrodes in microelectrophoresis only conduct
58 well (transform the flow of electrons from the current source to a flow of ions in solution) in solutions that
59 contain substantial Cl^- ions [7]. Accordingly, target cells can be located and subsequently their intracellular
60 electrical activity recorded with high signal to noise ratio and wide recording bandwidth (only for electrically
61 excitable cells, *i.e.*, neurons, muscle cells and some endocrine cells). Therefore, potassium chloride (KCl)
62 solution with concentration of 0.2 - 2 M is typically used to dissolve charged substances to be ejected [3,5].
63 The concentration of KCl should be as high as possible for low-noise intracellular recording while considering
64 the solubility of different substances. For nanoparticles, high KCl concentration significantly lowers their
65 repulsive energy barrier, *i.e.*, zeta potential at their hydrodynamic diameters, which leads to the irreversible
66 aggregation of nanoparticles [8]. This can cause blockages in the tip of micropipettes during ejection and thus
67 failed microelectrophoresis.
68

69 Secondly, to impale cells with minimal damage, a rule of thumb is that the outer diameter (OD) near the tip
70 of micropipettes should be less than 500 nm [3]. However, the inner diameter (ID) near the tip must be large
71 enough to allow the ejection of nanoparticles having comparable hydrodynamic diameters. Tips that are too
72 small will impede the ejection and subsequently cause the aggregation of nanoparticles in the tips, leading to
73 failed microelectrophoresis.

74

75 In this paper, we addressed these technical hurdles by preparing optimal nanoparticle suspensions with a
76 low KCl concentration and high pH to reach a compromise between the colloidal stability of nanoparticles for
77 ejection and high-fidelity intracellular recording. In addition, we fabricated micropipettes having appropriate tip
78 sizes to allow the intracellular delivery of nanoparticles into living cells with suitable ejecting current and
79 duration. These results suggest the future potential of microelectrophoresis as a simple and precise approach
80 in the intracellular delivery of various nanoparticles into the cellular environment.

81

82 **2 Materials and methods**

83

84 **2.1 QDs suspension preparation and colloidal stability measurement**

85

86 CdSe/ZnS core/shell structured QDs (emission maxima of 655 nm) with amine-derivatized polyethylene
87 glycol (PEG) surface functional group (Q21521MP; Invitrogen), hereafter referred to as 655-QDs, were used
88 to demonstrate intracellular microelectrophoresis. The KCl concentration and pH was adjusted by gradually
89 adding 2 M KCl, 0.1 M Hydrochloric Acid (HCl) or 0.1 M Sodium Hydroxide (NaOH) into QDs suspension in
90 fresh ultrapure water (concentration of QDs was consistently 10 nM). KCl, HCl and NaOH solutions were
91 centrifuged at 4000 revolutions per minute (rpm) for 1 minute before the addition to remove any large-size
92 impurities that can affect measurement results. Zetasizer nano ZSP (Malvern Instruments) was used for the
93 studies on the colloidal stability of 655-QDs as it can measure both the hydrodynamic size of the nanoparticles
94 *via* dynamic light scattering (DLS) and the zeta potential *via* laser Doppler electrophoresis in aqueous media
95 [9]. For the Zetasizer measurements, the Henry's function was set at the value of 1.50 [10]. The dispersant
96 was set to be water (Temperature: 25.0 °C; Viscosity: 0.8872 cP; Refractive Index: 1.330; Dielectric constant:
97 78.5) and its viscosity was used as the viscosity of the sample. The refractive index and absorption of 655-
98 QDs were set as 2.550 and 0.010 [11].

99

100 **2.2 Intracellular recording quality test**

101

102 To determine if the low KCl concentration that is necessary for maintaining the colloidal stability of
103 nanoparticles can permit high-fidelity intracellular recording, we compared the quality of intracellular recordings
104 acquired from dragonflies using standard 2 M KCl, 0.01 M KCl and optimized 655-QDs suspension. With their
105 large head capsule and ease of dissection, dragonflies are an ideal model system for recording *in vivo*,
106 intracellular activity. Wild-caught dragonflies (*Hemicordulia tau*) were immobilized with a mixture of beeswax
107 and gum rosin (solid form of resin) (1:1) on a plastic articulating stage as shown in **Figure 2A**. To gain the
108 access to the brain surface, a small hole was dissected on the posterior surface of the head capsule. A working
109 Ag/AgCl electrode (782500; A-M Systems) was connected to an intracellular bridge mode amplifier (BA-03X;
110 npi electronic) and a counter Ag/AgCl electrode was inserted into the head capsule surface to form a complete
111 electrical circuit. With a pipette holder (PPH-1P-BNC; ALA Scientific Instruments) and a micromanipulator
112 (MM-33; ALA Scientific Instruments), extremely fine-tipped glass micropipettes (pulled by program 1 in **Table**
113 **1**) were pierced into single lobula neurons. Neurons were stimulated by drifting small moving visual features
114 across a high refresh rate (165 Hz) LCD monitor placed directly in front of the dragonfly. Data were digitized
115 at 5 kHz with a 16-bit analog-to-digital converter and analyzed off-line with MATLAB. The visual stimulus
116 elicited voltage changes across the cell membranes and the digitized data indicated successful intracellular
117 neuronal recordings in real time.

118

119 **2.3 Micropipette fabrication**

120

121 P-97 Flaming/Brown type pipette puller (Sutter Instrument) was used to fabricate micropipettes from
122 aluminosilicate glass capillaries (30-0108; Harvard Apparatus). The pulling programs are listed in **Table 1**.
123 Micropipettes pulled by program 1 were used for intracellular recording on dragonflies. Micropipettes pulled by
124 program 2 were used for microelectrophoresis of QDs. To measure the tip IDs and ODs with high accuracy,
125 fabricated micropipettes were coated with a 3 nm-thick platinum film and fixed in two different orientations onto
126 scanning electron microscope (SEM) stubs: either vertically for tip IDs or horizontally for tip ODs measurement

127 under a FEI Quanta 450 FEG environmental SEM. Thus, it was not possible to measure both the ID and the
 128 OD for the same micropipette tip.

129
 130

Table 1 The parameters of pulling program 1 and 2 in P-97 puller.

Program		1	2	
Ramp		518	518	
Pressure		510	510	
Cycle	1	Heat	513	513
		Pull	0	0
		Velocity	8	8
		Time	1	1
	2	Heat	508	440
		Pull	100	100
		Velocity	65	65
		Time	100	100

131
 132
 133

2.4 Microelectrophoresis

134 Human embryonic kidney (HEK293) cells were seeded at 80,000 cells/dish onto a low-wall 35 mm imaging
 135 dish (80156; ibidi,) and cultured (37°C in a humidified incubator at 5% CO₂) for two days in 1 mL Dulbecco's
 136 modified Eagle's media (DMEM) supplemented with 2 mM L-glutamine and 10% fetal bovine serum. During
 137 electrophoresis, the media was changed to 2 mL DMEM supplemented with 25 mM HEPES (21063045;
 138 Thermo fisher) to maintain physiological pH in atmosphere at room temperature. As shown in **Figure 4A**,
 139 HEK293 cells (60-70% confluency) were visualized with 40X water immersion objective of a Nikon Ti-E
 140 inverted microscope equipped with cage incubator (Okolab). A stored aliquot of optimized QDs suspension
 141 was vortexed for 1 minute and sonicated from 4°C to 24°C without the use of external heat for 30 minutes to
 142 fully disperse QDs. The QDs suspension was carefully backfilled into micropipettes via a flexible plastic needle
 143 (Warner instruments). The micropipette was inserted with an Ag/AgCl working electrode from the blunt end
 144 and was held by a micromanipulator (Sensapex) to slowly move towards a single cell at a 50° angle. Another
 145 Ag/AgCl counter electrode was carefully placed into the media. The two electrodes were connected to the
 146 headstage of the intracellular bridge mode amplifier (BX-01; npi) to form a complete electrical circuit. A change
 147 in potential difference around -20 to -40 mV indicated that the tip of micropipette was successfully pierced
 148 through the cell membrane into the cytoplasm of the cell. A small current of -0.2 nA was then applied to eject
 149 QDs into the cell for 3 minutes.

150
 151

3 Results

152
 153
 154

3.1 Optimization of QDs suspension

155 The impact of KCl concentration on the colloidal stability of 655-QDs was investigated using particle size
 156 distribution (DLS technique) and zeta potential measurements. DLS measures the time-dependent fluctuation
 157 of scattered light intensity caused by the constant Brownian motion of particles, and reports their hydrodynamic
 158 diameters as the equivalent hydrodynamic diameters (D_H) of spheres that have the same average diffusion
 159 coefficient [12]. An established criterion for monodispersed nanoparticles is that their hydrodynamic diameters
 160 (D_H) should be less than twice of their diameters in the dry state (D_T) measured by transmission electron
 161 microscope (TEM) [13]. **Figure 1A** shows the image of 655-QDs (dark dots) on the surface of a TEM grid. The
 162 average shape of 655-QDs was modelled as a prolate ellipsoid with the major axis (a_T) of 9.7 ± 1.6 nm and
 163 the minor axis (b_T) of 6.7 ± 0.8 nm (± 1 standard deviation (SD), n = 82) rather than ideal spheres. Therefore,

164 as per the criterion for nanoparticle monodispersity in aqueous environment, monodispersed 655-QDs should
 165 theoretically have major hydrodynamic axes (a_H) in the range of 8.1 nm - 22.6 nm and minor hydrodynamic
 166 axes (b_H) in the range of 5.9 nm - 15.0 nm. To examine the monodispersity of elliptical 655-QDs based on the
 167 spherical hydrodynamic diameters reported by DLS technique, the following equation regarding the diffusion
 168 properties of anisotropic particles in Brownian motion [14], was used to translate the ellipsoidal dimensions
 169 (a_H and b_H) of 655-QDs to an equivalent diameter (D_H) of spheres having the same diffusion coefficient:
 170

$$D_H = 2 \times \frac{(a_H^2 - b_H^2)^{1/2}}{\ln \left(\frac{a_H + (a_H^2 - b_H^2)^{1/2}}{b_H} \right)}$$

171
 172 In view of the range of a_H and b_H dimensions, monodispersed 655-QDs were considered to have
 173 hydrodynamic diameters D_H over 13.2 nm and less than 35.0 nm.
 174

175 **Figure 1B** compares the scattered light intensity of particles across a range of sizes in 0.01 M and 2 M KCl
 176 solutions. The dotted lines indicate the size range of monodispersed 655-QDs from 13.2 to 35.0 nm. In 2 M
 177 KCl, QDs completely aggregated with a mean size around 1.5 μm due to the strong electrostatic screening
 178 effect caused by the high electrolyte concentration [8]. Whereas in 0.01 M KCl, only 59.2 % of the scattered
 179 light came from QDs aggregates or artefacts (*e.g.*, dust). Scattered light intensity is proportional to the sixth
 180 power of the particle radius and therefore the intensity-based size distribution is highly sensitive to very small
 181 numbers of aggregates or dust [15]. Thus, the number of QDs aggregates in 0.01M KCl was negligible
 182 compared to the total number of particles in the sample (determined using Mie theory, as shown in **Figure 1C**)
 183 [15]. Since the intensity-based size distribution is more reliable than number distribution, **Figure 1D** (red line)
 184 shows the change in the fraction of light intensity scattered by monodispersed 655-QDs (*i.e.*, portion of single
 185 QDs) with increasing KCl concentration. It sharply decreased from 40.8 % in 0.01 M KCl to 7.5 % in 0.1 M KCl.
 186 Note that there is no data on ultrapure water since the thickness of the electrical double layer of all particles is
 187 considered to be about 1 μm [16], making nanoscale particle size distribution measurement in solution *via* DLS
 188 impossible.
 189

190 The negative effect of KCl on the colloidal stability of 655-QDs revealed by DLS was also evidenced by
 191 zeta potential measurements. 655-QDs exhibited negative surface charge in ultrapure water, *i.e.*, 0 M KCl,
 192 leading to an average zeta potential of -29.9 mV (as shown in **Figure 1D**, blue line). Whereas with increasing
 193 KCl concentration, the zeta potential (colloidal stability of 655-QDs) rapidly approached zero due to the
 194 stronger electrostatic screening effect [8]. The zeta potential of -29.9 mV for 0 M KCl agrees with a previous
 195 report on the zeta potential of gold nanoparticles that are also surface-functionalized with amine-derivatized
 196 PEG [17].
 197

198 The measurements of the zeta potential and size distribution of 655-QDs in different KCl solutions (**Figure**
 199 **1D**) show that a KCl concentration as low as 0.01 M is most suitable for achieving high zeta potential (absolute
 200 value), which is essential to maintain colloidal stability. However, the zeta potential of -7.4 mV for 655-QDs in
 201 0.01 M KCl solution is still not sufficiently high (absolute value) considering that particles with zeta potential
 202 more positive than 30 mV or more negative than -30 mV are generally considered to represent sufficient
 203 repulsion to maintain their colloidal stability [9]. Thus, we investigated the effect of pH adjustment on the zeta
 204 potential of 655-QDs and evaluated its capability to further stabilize 655-QDs.
 205

206 We commenced with testing impact of pH for QDs suspended in ultrapure water, *i.e.*, 0 M KCl (**Figure 1E**,
 207 black line). The as-prepared QD suspension (without pH adjustment) had a pH of ~ 7 and a zeta potential of -
 208 16.6 mV. Note that this zeta potential value (-16.6 mV) was different to that of the QD suspension in ultrapure
 209 water used for the study of the impact of KCl concentration (-29.9 mV). This difference was attributed to the
 210 large uncertainty of zeta potential measurements in ultrapure water due to low conductivity. The increase of
 211 the pH by addition of alkali (NaOH) resulted in a more negative charge for 655-QDs particles (decreased zeta

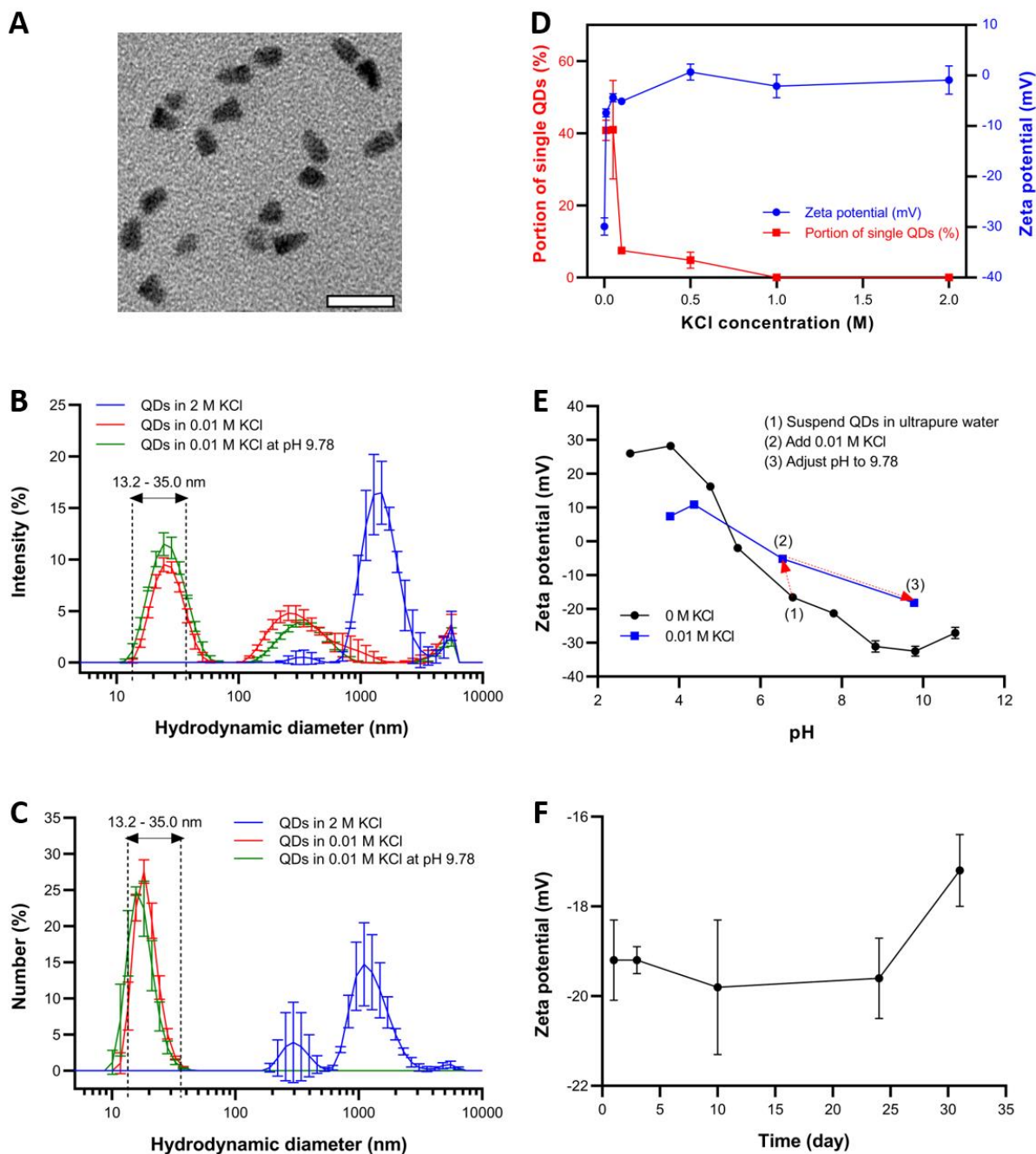


Figure 1 (A) TEM image of 655-QDs reveals an average shape of prolate ellipsoid with a major axis (a_T) of 9.7 ± 1.6 nm and a minor axis (b_T) of 6.7 ± 0.8 nm (± 1 SD with $n = 82$). Scale bar, 25 nm. (B) the size distribution by intensity and (C) by number of 655-QDs in 2 M KCl (pH 5.21), 0.01 M (pH 6.55) and optimized suspensions (0.01 M KCl adjusted to pH 9.78). Each data point comprises 12 repeat measurements of 3 independent samples (Error bars, ± 1 SD with $n = 3$). The dot lines indicate the size range of monodispersed 655-QDs from 13.2 to 35.0 nm. (D) the zeta potential of 655-QDs and the portion of single QDs (determined as fraction of light intensity scattered by monodispersed 655-QDs) as a function of KCl concentration. Error bars, ± 1 SD with $n = 3$. (E) the zeta potential of 655-QDs in ultrapure water and 0.01 M KCl solution with different pH values. Error bars, ± 1 SD with $n = 3$. Inserted with each step of the optimal preparation process of 655-QDs suspension for microelectrophoresis. (F) the stability of 655-QDs zeta potential in optimized suspension. Error bars, ± 1 SD with $n = 3$.

212 potential). Conversely, the decrease of the pH by addition of acid (HCl) increased the zeta potential. The most
 213 stable state of 655-QDs was achieved by adjusting the pH of QDs suspension to 9.81, where the maximal zeta

214 potential (absolute value) of -32.5 mV was obtained.

215

216 Next, we investigated the impact of pH for QDs suspended in 0.01 M KCl solution (**Figure 1E**, blue line).
217 Without pH adjustment, the QD suspension had a zeta potential of -5.2 mV and a pH of 6.55. For lower pH of
218 3.78 and 4.37, the zeta potential increased to +7.4 and +10.9 mV, respectively. For higher pH of 9.78, the zeta
219 potential decreased to -18.2 mV. These results show that both lower and higher pH can enhance the absolute
220 value of the zeta potential and thus the colloidal stability compared to the QD suspension without pH
221 adjustment. Thus, pH adjustment can effectively buffer the negative effect of 0.01 M KCl on the stability of
222 655-QDs.

223

224 Although a stable state of 655-QDs also exists at acid pH, a strong acid environment ($\text{pH} < 4$) is not
225 recommended by the supplier, as the polymer coating can dissociate, exposing and dissolving the core/shell
226 structure. In addition, due to the high mobility of hydrogen ions (H^+), a large amount of H^+ in
227 microelectrophoresis can result in lowering of the pH in the vicinity of the tip of micropipettes [18]. This localized
228 change in pH has been proposed to excite the cell undergoing intracellular recording and interfere with the
229 normal physiological state [19]. On the contrary, 655-QDs do not degrade in a strong basic environment ($\text{pH} > 9$)
230 as noted by the supplier. Furthermore, in comparison to the electrophoretic mobility of H^+ ($36.25 \mu\text{m cm/Vs}$ in
231 water at $25.0 \text{ }^\circ\text{C}$), hydroxide ion (OH^-) has a lower electrophoretic mobility ($20.50 \mu\text{m cm/Vs}$ in water at 25.0
232 $^\circ\text{C}$), resulting in less effect on the intracellular activity [20].

233

234 Based on the investigation of KCl concentration and pH adjustment on the colloidal stability of QDs, we
235 established the following optimal protocol for the preparation of QDs suspension for microelectrophoresis. The
236 method is to initially dilute QDs stock solution with fresh ultrapure water to 10 nM and then gradually add 2 M
237 KCl to the suspension until a final KCl concentration of 0.01 M achieved. Finally, the pH is adjusted to 9.78 by
238 gradually adding freshly prepared 0.1 M NaOH to further stabilize QDs (indicated by dashed red lines with
239 arrow in **Figure 1E**). The green curve in **Figure 1B** shows the size distribution of optimized 655-QDs
240 suspension, where 53.9 % of scattered light comes from monodispersed QDs that constitute 91.4 % of the
241 total number of particles in the sample as **Figure 1C** shows.

242

243 For practical microelectrophoresis applications, preparation of fresh suspensions would be too time-
244 consuming. A stock suspension with good colloidal stability and ready for use would be highly beneficial.
245 **Figure 1F** shows the shelf life of optimized 655-QDs suspensions (0.01 M KCl at pH 9.78). They were aliquoted
246 and stored at $4.0 \text{ }^\circ\text{C}$ in dark. The zeta potential values of QDs in these intact aliquots were measured on
247 different days, which remained the same for at least 24 days, indicative of this beneficial, long-term colloidal
248 stability.

249

250 **3.2 The effect of KCl concentration on the quality of intracellular recording**

251

252 The highest KCl concentration suitable to maintain colloidal stability of QDs was determined to be 0.01 M,
253 which raised the problem whether such a low electrolyte concentration and the existence of 655-QDs in
254 optimized suspensions allow for the recording of intracellular activity with sufficiently high fidelity in real-time.
255 Thus, we compared the quality of intracellular recordings acquired by 2 M KCl solution (used in standard
256 dragonfly electrophysiology) with those of 0.01 M KCl solution and optimized 655-QDs suspension (0.01 M
257 KCl at pH 9.78). The intracellular recordings were captured from visual neurons, binocular small target motion
258 detector (BSTMD2), in the optic lobes of living dragonflies [21]. When BSTMD2 is presented with a small
259 drifting target, the cell responds by significantly increasing the frequency of action potential firing.

260

261 **Figure 2B** shows the typical raw responses (left panel) and an enlarged view of individual spike waveforms
262 (right panel) recorded by 2 M KCl, 0.01 M KCl and optimized 655-QDs suspension from BSTMD2 cells ($n = 6$)
263 presented with a small moving target. The average tip resistance for micropipettes filled with 2 M KCl, 0.01 M
264 KCl and optimized 655-QDs suspension was $120 \text{ M}\Omega$, $335 \text{ M}\Omega$ and $300 \text{ M}\Omega$, respectively. Although the
265 recordings acquired by using low KCl concentration (0.01 M KCl without QDs and optimized 655-QDs

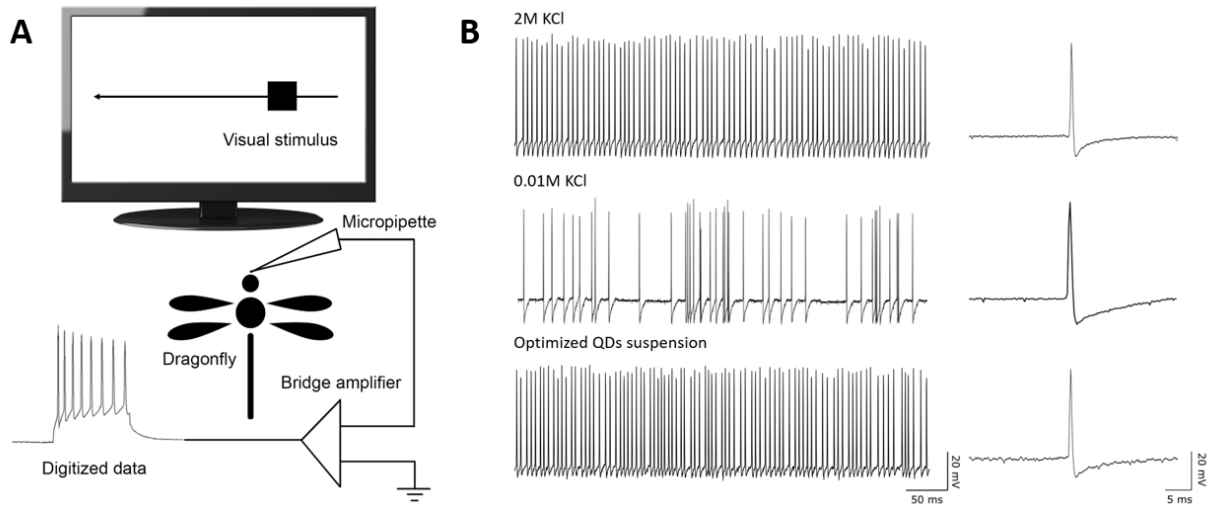


Figure 2 (A) schematic illustration of the experiment setup for intracellular recording of dragonflies. A liquid crystal display (LCD) monitor was placed in front of the dragonfly for stimulating visual neurons by drifting small moving objects. The visual stimulus elicited voltage changes across the cell membranes of single lobula neurons, which were recorded in real-time. **(B)** the responses of two BSTMD2 cells in two separate dragonflies to the presentation of a drifting object, which were recorded with micropipettes filled with 2 M KCl solution, 0.01M KCl solution and optimized 655-QDs suspension (0.01 M KCl at pH 9.78).

266 suspension) had a greater degree of variation in quality (*i.e.*, noise and signal amplitude) than the recordings
 267 acquired by 2 M KCl, it was possible to count spikes that were distinct from the resting potential without any
 268 issue in temporal responsiveness. In addition, spiking responses and individual action potential waveforms
 269 remained very similar for all cases.

270

271 As a conclusion, KCl concentration of 0.01 M and the existence of 655-QDs in suspensions can precisely
 272 locate target cells, and then produce high-fidelity intracellular recordings.

273

274 3.3 Optimizing the tip size of micropipette for intracellular delivery

275

276 For successful microelectrophoresis, the tip ID of the micropipette is required to be larger than the sum of
 277 hydrodynamic diameters of nanoparticles and other dissolved ions that pass through the tip for conductivity.
 278 The range of hydrodynamic diameter of monodispersed 655-QDs is 13.2 - 35.0 nm. The theoretical hydrated
 279 diameters of K⁺, Cl⁻ and Na⁺ ions are 0.3, 0.4 and 0.2 nm, respectively [22]. Considering the unavoidable trace
 280 amount of QDs aggregates or artefacts (*e.g.*, dust) existing in the optimized QDs suspension (**Figure 1B**), the
 281 tip ID of the micropipette should be as large as possible to eliminate tip blockage. However, as proposed by
 282 previous studies, the tip OD should be less than 500 nm to avoid physical damage to living cells [3]. To achieve
 283 small tip OD yet large enough tip ID, we chose aluminosilicate glass for the fabrication of micropipettes since
 284 a unique characteristic of aluminosilicate micropipettes is that the ratio of their ID to OD increases remarkably
 285 towards the tip [23]. Thus, they have extremely thin wall near the tip, which provides the smallest possible tip
 286 OD to avoid physical damage to cells.

287

288 The pulling program 1 listed in **Table 1** was designed to fabricate micropipettes with tip ID of *ca.* 100 nm in
 289 previous studies of standard dragonfly electrophysiology [24]. To achieve larger tip ID suitable for QDs ejection,
 290 we reduced the heat value in the second cycle from 508 in program 1 to 440 in program 2. **Figure 3** shows
 291 the SEM images of aluminosilicate micropipettes pulled by program 2 in front and side views. The average tip
 292 OD of 26 fabricated micropipettes was 202 nm with a tolerance of ± 35 nm (± 1 SD). The average tip ID of
 293 another 26 micropipettes was 206 nm with a larger tolerance of ± 46 nm (± 1 SD). These two averages were
 294 nearly identical, which validated the unique characteristics of aluminosilicate micropipettes. Their extremely
 295 thin wall near the tip made the tip OD as small as possible to minimize the physical damage to cell membrane
 296 while having large enough tip ID for the ejection. The average tip ID of approx. 200 nm was the maximum

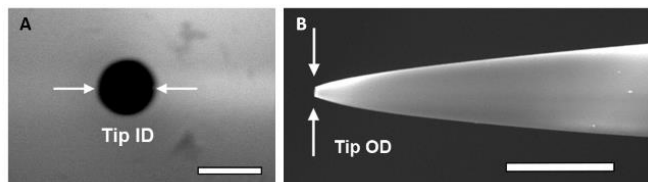


Figure 3 (A) high resolution SEM image of a micropipette for microelectrophoresis of 655-QDs with a tip ID of 211 nm (front view). The orifice of micropipette is the black circle near the centre of the image. Scale bar, 250 nm. (B) high resolution SEM image of another micropipette (pulled with program 2) with a tip OD of 212 nm (side view). Scale bar, 2.5 μ m.

297 achievable size by lowering the heat value in the second cycle. For lower heat values, the aluminosilicate
 298 capillaries did not soften sufficiently to form micropipettes. The variance was in part caused by the
 299 observational error due to the inconsistency of pipette angle when manually fixing micropipettes onto the
 300 vertical SEM sample holder. In addition, when pulling micropipettes, capillaries with slightly different IDs (0.52
 301 ± 0.03 mm, ± 1 SD, $n=26$) and ODs (0.99 ± 0.02 mm, ± 1 SD, $n=26$), had different distances to the box heating
 302 filament and different volume of air enclosed in the internal channel, which altered the glass temperature and
 303 resulted in variations in tip ID and OD of micropipettes [25].

304
 305 In summary, the range of tip IDs of our aluminosilicate micropipettes is suitable for the ejection of 655-QDs
 306 and the tip ODs are less than 500 nm to avoid physical damage to cells as proposed by previous studies [3].
 307

3.4 Successful cytoplasmic delivery of QDs into living cells *via* microelectrophoresis

308
 309
 310 **Figure 4B** shows the differential interference contrast (DIC), fluorescent and overlay images of the typical
 311 results after microelectrophoresis delivery of 655-QDs into HEK cells ($n=20$). QDs evenly dispersed throughout
 312 the cytoplasm without entering the nucleus. During microelectrophoresis, the resistance of micropipettes was
 313 frequently measured to confirm that there was no blockage or breakage in the tips. The resistance of several
 314 micropipettes varied from 50 M Ω to 80 M Ω due to the variation in their tip sizes and remained the same when
 315 removed out of the cells after delivery, which indicated that there was no tip blockage or breakage happened
 316 during microelectrophoresis.
 317

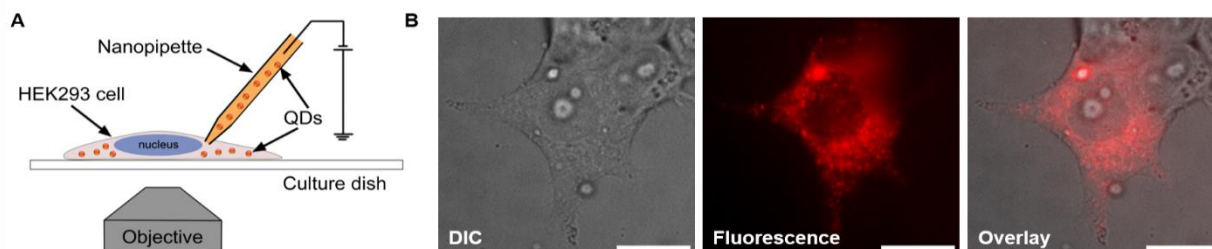


Figure 4 (A) diagram of microelectrophoresis of 655-QDs into HEK293 cells. (B) DIC, fluorescence, and overlay images of a HEK293 cell with microelectrophoretic-delivered 655-QDs. The red dots in the cytoplasm are 655-QDs. Scale bar, 10 μ m.

318 4 Concluding remarks

319
 320 We demonstrated for the first time the use of the well-established microelectrophoresis technique for the
 321 successful delivery of nanoparticles, such as QDs used here, into the cytoplasm of living cells. This was
 322 achieved by overcoming the following two critical challenges. Firstly, we prepared QDs suspensions with low
 323 KCl concentration and high pH value, which maintained high QDs colloidal stability to prevent aggregation and
 324 blockages in the tip of micropipettes during ejection, while being able to record the intracellular electrical activity
 325 of dragonfly neurons with high fidelity. Secondly, we fabricated micropipettes with inner tip diameters of approx.
 326 200 nm, which was large enough to allow the ejection of QDs and less than 500 nm to avoid physical damage
 327 to HEK293 cells as proposed by previous studies [3]. This successful microelectrophoretic ejection of QDs
 328 lays the foundation for further studies and applications of microelectrophoresis technique for the intracellular
 329 delivery of various nanoparticles.
 330

331 This work was performed in part at the Optofab node of the Australian National Fabrication Facility (ANFF)
332 utilizing Commonwealth and SA State Government funding. The authors acknowledge partial support from the
333 Australian Research Council Centre of Excellence for Nanoscale BioPhotonics (CNBP) (CE140100003) and
334 Discovery Early Career Researcher Award (DECRA) from Australian Research Council (ARC)
335 (DE150100548). M.H. thanks K. Neubauer, A. Slattery and J. Sibbons for their assistance in SEM, TEM, live
336 cell microscopy at Adelaide Microscopy.

337

338 The authors have declared no conflict of interest.

339

340 The data that support the findings of this study are available from the corresponding author upon reasonable
341 request.

342

343 5 References

344

- 345 [1] Stewart, M. P., Sharei, A., Ding, X., Sahay, G., Langer, R., Jensen, K. F., *Nature* 2016, 538, 183-192.
346 [2] Chou, L. Y., Ming, K., Chan, W. C., *Chem. Soc. Rev.* 2011, 40, 233-245.
347 [3] Curtis, D. R., *Microelectrophoresis*, New York: Academic Press, 1964.
348 [4] Tekle, E., Astumian, R. D., Chock, P. B., *Biochem. Biophys. Res. Commun.* 1990, 172, 282-287.
349 [5] Mobbs, P., Becker, D., Williamson, R., Bate, M., Warner, A., Techniques for dye injection and cell labelling, in
350 Proceedings of the *Microelectrode techniques. The Plymouth workshop handbook*. Cambridge, UK: The Company of Biologists
351 Ltd, 1994, 361-387.
352 [6] Lalley, P. M., U. Windhorst, H. Johansson (Eds.), in: *Modern Techniques in Neuroscience Research*, Springer Berlin
353 Heidelberg, Berlin, Heidelberg 1999, p. 193-212.
354 [7] Axon Instruments, I., *The Axon guide for electrophysiology & biophysics laboratory techniques*, Axon Instruments,
355 1993.
356 [8] Zhang, W., in: *Nanomaterial: Advances in Experimental Medicine and Biology* 2014, p. 19-43.
357 [9] Clogston, J. D., Patri, A. K., S.E. McNeil (Ed.), in: *Characterization of Nanoparticles Intended for Drug Delivery*, Humana
358 Press, Totowa, NJ 2011, p. 63-70.
359 [10] Henry, D., The cataphoresis of suspended particles. Part I. The equation of cataphoresis, in Proceedings of the
360 *Proceedings of the Royal Society of London A: Mathematical, Physical and Engineering Sciences*, 1931, 133, 106-129.
361 [11] Hondow, N., Brydson, R., Wang, P., Holton, M. D., Brown, M. R., Rees, P., Summers, H. D., Brown, A., *J. Nanopart. Res.*
362 2012, 14, 1-15.
363 [12] Pecora, R., *Dynamic light scattering: applications of photon correlation spectroscopy*, Springer Science & Business
364 Media, 2013.
365 [13] Moon, J., Choi, K.-S., Kim, B., Yoon, K.-H., Seong, T.-Y., Woo, K., *J. Phys. Chem. C* 2009, 113, 7114-7119.
366 [14] Perrin, F., *J. Phys. Radium* 1936, 7, 1-11.
367 [15] Mie, G., *Ann. Phys. (Berlin, Ger.)* 1908, 330, 377-445.
368 [16] Israelachvili, J. N., *Intermolecular and surface forces*, Academic press, 2011.
369 [17] Xia, X., Yang, M., Wang, Y., Zheng, Y., Li, Q., Chen, J., Xia, Y., *ACS Nano* 2012, 6, 512-522.
370 [18] Gruol, D. L., Barker, J. L., Huang, L. Y., MacDonald, J. F., Smith, T. G., Jr., *Brain Res* 1980, 183, 247-252.
371 [19] Frederickson, R. C., Jordan, L. M., Phillis, J. W., *Brain Res* 1971, 35, 556-560.
372 [20] Duso, A. B., Chen, D. D. Y., *Anal. Chem.* 2002, 74, 2938-2942.
373 [21] O'Carroll, D., *Nature* 1993, 362, 541-543.
374 [22] Marcus, Y., *Chem. Rev.* 1988, 88, 1475-1498.
375 [23] Instrument, S., *P-97 Pipette Cookbook*, 2008.
376 [24] O'Carroll, D. C., Biomimetic visual detection based on insect neurobiology, in Proceedings of the *Electronics and*
377 *Structures for MEMS II*, 2001, 4591, 1-11.
378 [25] Chen, M. J., Stokes, Y. M., Buchak, P., Crowdy, D. G., Foo, H. T., Dowler, A., Ebandorff-Heidepriem, H., *Opt. Mater.*
379 *Express* 2016, 6, 166-180.

380